MINERALOGICAL MAGAZINE, DECEMBER 1983, VOL. 47, PP. 527-38

Deformation and recrystallization of pyrite

K. R. McCLAY AND P. G. ELLIS

Geology Department, University of London, Goldsmiths' College, Rachel McMillan Building, Creek Road, Deptford, London SE8 3BU

ABSTRACT. A detailed study of pyrite in a number of metamorphosed, stratiform, sediment-hosted Pb–Zn deposits has shown the importance of cataclastic deformation, pressure-solution, and grain growth in the deformation and textural development of pyrite. Primary depositional or early diagenetic microstructures are preserved in pyritic ores deformed or metamorphosed at grades up to mid-upper greenschist facies, whereas at higher temperatures only metablastic or annealed pyrite textures are found. Brittle deformation is found at all metamorphic grades and is favoured by coarse grain-sizes. Pressure-solution is a major deformation mechanism in fine-grained pyritic ores in low-grade metamorphic environments. Grain growth and annealing dominate at higher metamorphic temperatures and are likely to have obliterated any evidence of deformation by dislocation processes. Significant macroscopic ductility of fine-grained pyritic ores in low-grade environments may be accounted for by a combination of pressure-solution, grain boundary sliding, and cataclastic flow.

PYRITE has traditionally been considered to be an extremely brittle mineral during deformation and metamorphism. In many metamorphosed and deformed sulphide deposits, pyrite exhibits cataclastic textures (Vokes, 1969, 1971; Ramdohr, 1969; Mookherjee, 1976; Sarkar *et al.*, 1980). Mookherjee (1971), however, noted that in some instances pyrite could possibly undergo plastic deformation and this is discussed further by Sarkar *et al.* (1980).

Experimental deformation of pyrite has consistently been in the brittle deformation field (Adams, 1910; Buerger, 1928; Newhouse and Flaherty, 1930; Bridgman, 1937; Robertson, 1955; Lang, 1968; Graf and Skinner, 1970; Atkinson, 1972, 1975) for temperatures up to 400 °C, strain rates of 10^{-4} to 10^{-7} sec^{-1}, and confining pressures up to 1000 MPa. From the results of experiments on wet pyrite Atkinson (1972) suggested that solution mass transfer may be an important mechanism during natural deformation. Recent experimental deformation of pyrite at temperatures up to 700 °C (Cox *et al.*, 1981) and re-evaluation of earlier work (Graf *et al.*, 1981) has demonstrated that pyrite can deform by dislocation processes. In addition, recent transmission electron microscope studies of naturally deformed pyrite by Couderc *et al.* (1980) have also demonstrated that pyrite can deform by dislocation processes.

In some sulphide deposits which have undergone relatively low-grade metamorphism and deformation (e.g. Mount Isa, Australia; Cirque and Tom, Canada), pyrite-rich units can exhibit significant macroscopic ductility with the development of folds and shear zones (McClay, 1978, 1979). The macroscopic ductility is achieved without apparent significant intra-crystalline plasticity.

This paper examines the deformation and metamorphism of pyrite in a number of stratiform, sediment-hosted Pb–Zn deposits (fig. 1, Table I). Grain-size data and microstructural data have been obtained for pyrite-rich units from a number of the deposits cited in this study. Significant textural and grain-size variations are found and these are interpreted in the light of changes in deformation and recrystallization mechanisms during prograde metamorphism. These results are compared with those obtained from experimentally deformed pyrite and incorporated into a proposed deformation mechanism map for pyrite.

Stratiform sulphide deposits discussed in this study

The sediment-hosted, stratiform sulphide deposits discussed in this study all contain, or are associated with, pyrite-rich units. All of the deposits, with the exception of Mount Isa (included to complete a prograde metamorphic sequence of deformed sulphide deposits), are located in the Canadian Cordillera (fig. 1). This suite of deposits encompasses the following metamorphic grades:

(*a*) Very low grade (sub-greenschist facies). The Selwyn Basin–Kechika Trough black clastic-hosted barite–lead–zinc mineralization of the Driftpile, Cirque, and Tom deposits (figs. 1 and 2).

(*b*) Low greenschist facies. The Mount Isa silver–lead–zinc deposit.

(*c*) Mid-upper greenschist facies. The Sullivan deposit (figs. 1 and 2, Table I) and the Reeves MacDonald deposit (fig. 1).

(*d*) Amphibolite facies. The Faro deposit (Templeman-Kluit, 1970; Campbell and Ethier, 1974) and Kootenay Arc-type deposits (Höy, 1982) such as the HB mine (Fyles, 1970) (figs. 1 and 2).

(*e*) Upper amphibolite facies. The Shuswap type deposits such as the It and King Fissure mineralization (figs. 1 and 2).

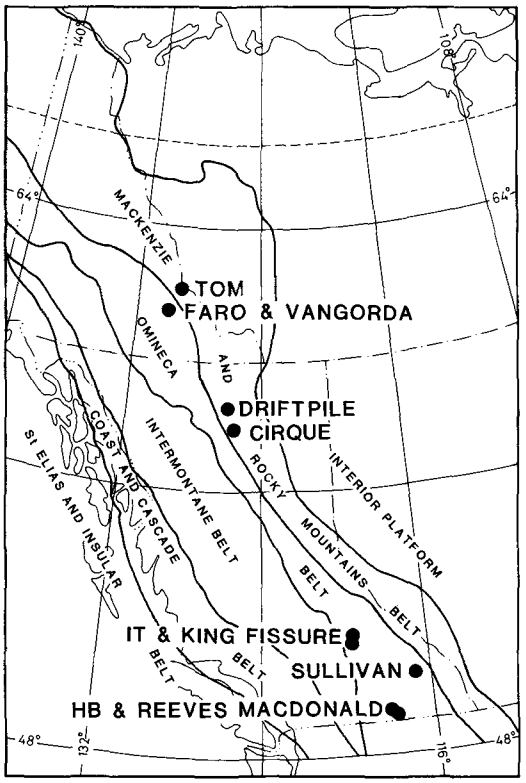

FIG. 1. Location of sediment-hosted stratiform sulphide deposits in the Canadian Cordillera.

Details of these deposits are given in Table I. Data from the Vangorda, It, and King Fissure deposits are included from Templeman-Kluit (1970) for comparison and to encompass very high-grade metamorphism.

All of the deposits cited occur in deformed terrains with at least one cleavage/foliation developed. The approximate *P/T* fields for the metamorphism of these deposits are shown in fig. 2. It is beyond the scope of this paper to give a detailed résumé of the geological histories of these deposits. They have been well documented and further details can be obtained from the references given in Table I.

In this study, detailed grain-size measurements, textural and microstructural studies have been carried out on hand specimens which, in the case of a number of the deposits, were collected during the course of detailed structural mapping (McClay, 1979, 1982, 1983).

Pyrite deformation mechanisms

Experimental deformation. Early experimental studies on both single crystals and polycrystalline pyrite were found to occur wholly in the brittle, or brittle/ductile fields (Adams, 1910; Buerger, 1928; Newhouse and Flaherty, 1930; and Bridgman, 1937).

Robertson (1955) showed that in single crystals

TABLE I. *Deposits discussed in this study*

Deposit	Locality	Metamorphic grade	Index mineral	Ore mineralogy	References
Tom	Yukon, Canada	Sub-Greenschist	—	Baryte, sphalerite, galena, pyrite	Large (1980), McClay (1983)
Driftpile	NE British Columbia, Canada	Sub-Greenschist	—	Baryte, sphalerite, pyrite	MacIntyre (1979)
Cirque	NE British Columbia, Canada	Sub-Greenschist	—	Barite, sphalerite, pyrite, galena	MacIntyre (1979), Jefferson *et al.* (1983)
Mount Isa	NW Queensland, Australia	Low Greenschist	Chlorite	Galena, sphalerite, Pyrrhotite, pyrite	Mathias and Clarke (1975) McClay (1979)
Sullivan	SE British Columbia, Canada	Mid Greenschist	Biotite/Chlorite	Galena, sphalerite, pyrrhotite, pyrite	Hamilton *et al.* (1982) Hamilton *et al.* (1983)
Vangorda	Yukon, Canada	Mid Greenschist	Biotite/Chlorite	Pyrite, galena, sphalerite	Templeman-Kluit (1970) Campbell and Ethier (1974)
Reeves MacDonald	SE British Columbia, Canada	Mid–upper greenschist	Biotite	Pyrite, galena, sphalerite	Fyles and Hewlett (1959)
HB	SE British Columbia, Canada	Amphibolite	Biotite/garnet	Pyrite, galena, sphalerite	Fyles and Hewlett (1959)
FARO	Yukon, Canada	Amphibolite	Biotite/garnet	Pyrite, galena, sphalerite	Templeman-Kluit (1970) Campbell and Ethier (1974)
It	British Columbia, Canada	Upper amphibolite	Sillimanite	Pyrite, galena, sphalerite	Templeman-Kluit (1970) Fyles (1970)
King Fissure	British Columbia, Canada	Upper amphibolite	Sillimanite	Pyrite, galena, sphalerite	Templeman-Kluit (1970) Fyles (1970)

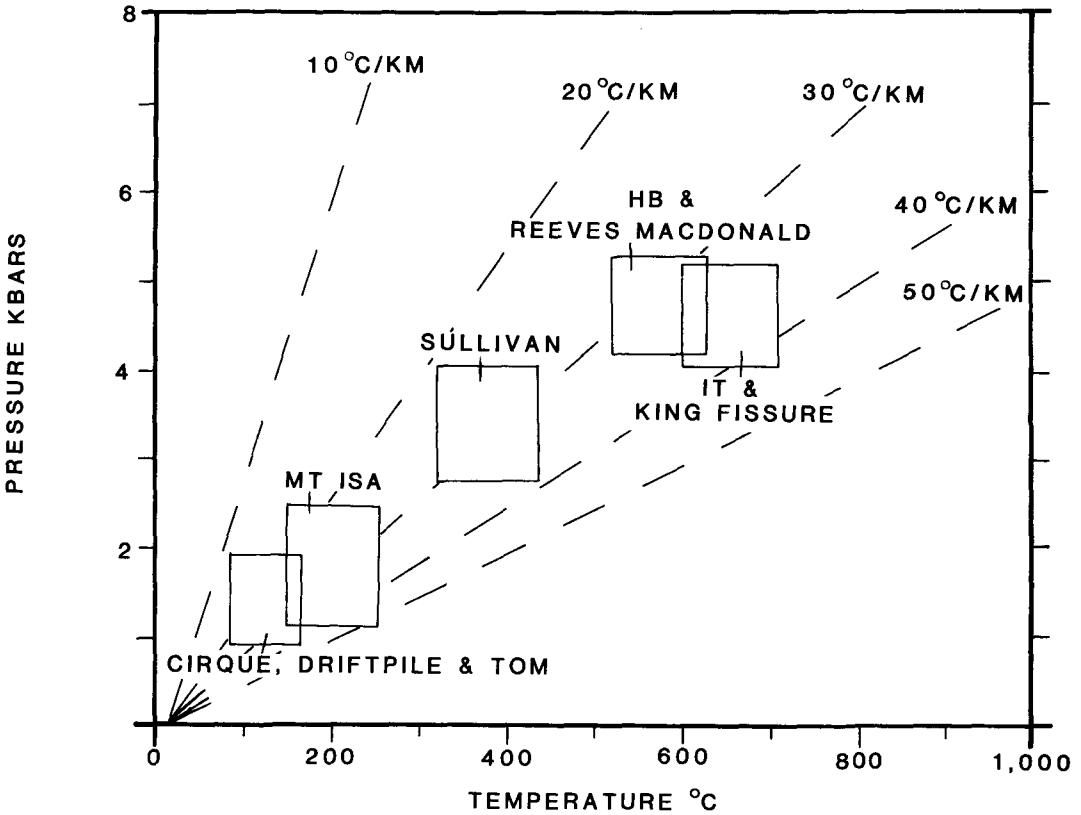

FIG. 2. Approximate pressure–temperature fields for the metamorphism of the sulphide deposits discussed in this study. The fields are based on our own data and that published in the references cited in the text and Table I.

of pyrite the ultimate strength increases with increasing confining pressure. Lang (1968) showed a similar relation with polycrystalline pyrite, even at extremely high (600 MPa.) confining pressures. Similar brittle failure was found by Graf and Skinner (1970) on single crystals at temperatures up to 650 °C, strain-rates of 7.8×10^{-5} sec^{-1} to 7.8×10^{-7} sec^{-1}, and confining pressures of 1000 MPa.

Atkinson (1972, 1975) using dry polycrystalline pyrite under temperatures of 20 to 400 °C, confining pressures of 100 to 300 MPa and strain-rates of 10^{-4} to 10^{-7} sec^{-1}, found deformation in the brittle and brittle/ductile fields. However, the specimens showed only cataclastic textures with large scale fractures, with accretionary steps, similar to those found by Gay (1970) in marble, gneiss and quartzite. In no experiment was evidence found of plastic deformation. Atkinson (1972) concluded that any ductile deformation was achieved by cataclastic flow.

In recent experimental deformation of pyrite at temperatures above 450 °C, confining pressures of 300 MPa, and varying strain-rates of 2×10^{-4} to 2×10^{-5} sec^{-1} Cox *et al.* (1981) found that polycrystalline pyrite was able to undergo up to 20% shortening. The specimens characteristically showed grain boundary bulging, grain elongation and deformation bands, which at the highest strains underwent recrystallization. Below 650 °C there is an increase in dislocation density, with the formation of dislocation walls, effectively work hardening the specimen. Above 650 °C dislocation climb becomes common and leads to dynamic recovery and recrystallization, and to steady state flow. Cox *et al.* (1981) also describe small sites of intragranular recrystallization, commonly between pairs of deformation band boundaries. They conclude that dislocation flow in pyrite is a more thermally activated process, with a higher activation enthalpy (100–110 kcal/mole at 500–600 °C) than other common sulphides such as galena and sphalerite.

A re-evaluation of Graf and Skinner's (1970)

work by Graf *et al.* (1981) has shown that the strains achieved before brittle failure in some of the high-temperature experiments were plastic in nature, involving dislocation movement. The experiments of Graf and Skinner (1970) were therefore in the brittle-ductile transition.

However, it must be pointed out that the experimental deformation of pyrite indicates significant work hardening during plastic deformation (Cox *et al.*, 1981).

Natural deformation. In many naturally deformed sulphide orebodies pyrite typically exhibits cataclastic deformation textures (Vokes, 1969, 1976; Ramdohr 1969; Davies, 1972) or thermal annealing textures (Lawrence, 1972; Rozendaal, 1978).

Mookherjee (1971), however, suggested that the bending of some pyrite crystals indicates plastic deformation. Other studies (Natale, 1971; Couderc *et al.*, 1980), particularly using Transmission Electron Microscopy (TEM) have demonstrated that plastic deformation involving dislocation movement can occur in naturally deformed pyrite.

In addition, textural evidence from detailed microstructural studies (McClay, 1978) suggests that pyrite can undergo deformation by pressure-solution (i.e. diffusive mass transfer). These features are described in detail in this paper. Pyrite solubility increases with an increase in temperature and a decrease in pH with only a slight change in solubility with different solution compositions (Barnes and Czamanske, 1967). Masalovich (1977) found a sharp increase in pyrite solubility at temperatures of 300 to 350 °C.

This work and other research on pyrite solubility suggests that under many geological conditions, pyrite may undergo deformation by pressure-solution.

Pyrite slip systems. The slip systems of pyrite are not well understood, although the most recent studies (Levade *et al.*, 1979; Couderc *et al.*, 1980; Graf *et al.*, 1981) have demonstrated the operation of the {100} ⟨001⟩ system. Van Goethem *et al.* (1978) propose the {100} ⟨011⟩ slip system. Only Arnold (1978) proposes the additional slip systems {111}, {021}, and {110}. However, these additional slip systems are not confirmed by Couderc *et al.* (1980) in their work from the same locality. The structure of pyrite is closely related to that of NaCl, being modified by a pair of covalently bonded sulphur atoms (Van Goethem *et al.*, 1978). As a result pyrite slip systems are different from those in the NaCl-type structure where glide is predominantly on the {110} ⟨1$\bar{1}$0⟩ system.

Cox *et al.* (1981) have proposed that three possible slip systems may operate in pyrite—{100} ⟨001⟩, {100} ⟨011⟩, and {110} ⟨1$\bar{1}$0⟩.

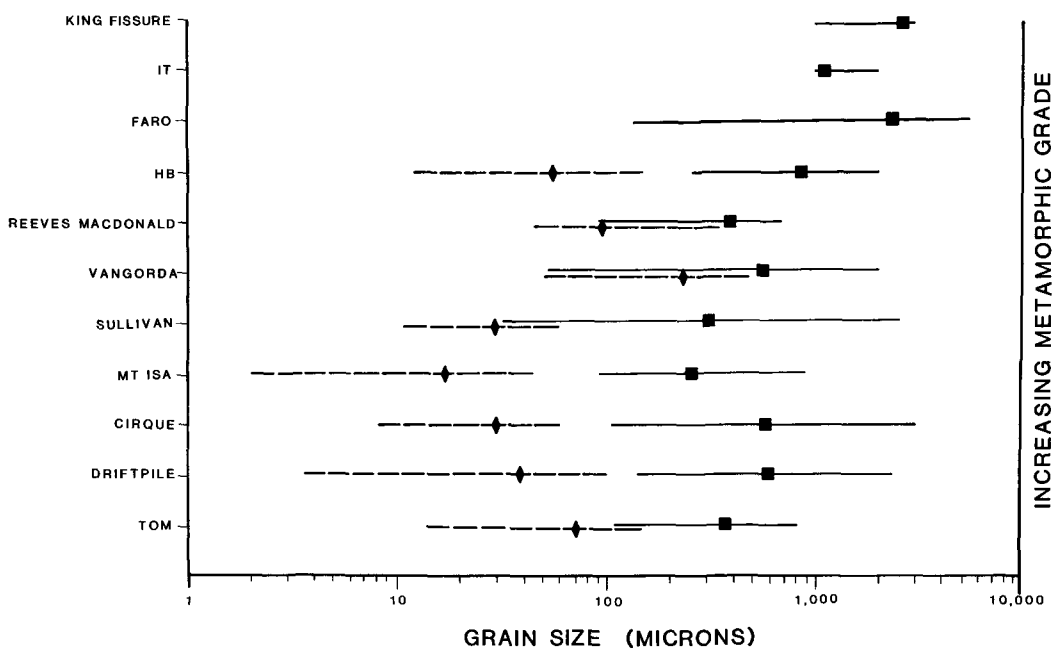

FIG. 3. Pyrite grain-size data. Dashed lines with a diamond symbol indicate the range and mean of early-primary pyrite phases, solid lines with a square symbol indicate the range and mean of metamorphic pyrite grain-sizes. Data for the Vangorda, It and King Fissure deposits are taken from Templeman-Kluit (1970).

Grain-size data

Pyrite grain-size data have been collected from most of the deposits discussed in this study (fig. 3). In general there is a crude correlation between an increase in pyrite grain-size and an increase in metamorphic grade (Templeman-Kluit, 1970). In detail, however, the pyrite grain-size will also depend on a number of other factors, in particular the initial grain-size prior to metamorphism. The factors which affect pyrite grain-size in a metamorphosed sulphide deposit may be assessed in terms of first-order and second-order effects.

First-order factors. These are factors which are considered to have a dominant control on pyrite grain-sizes. They may be further subdivided into primary/depositional effects and post-depositional/metamorphic effects. Primary/depositional structures include primary euhedral pyrite grains, spheroids, aggregates of spheroids and colloform textured pyrite, and diagenetic pyrite overgrowths (commonly euhedral). The grain-size of these depositional/diagenetic structures can be expected to strongly influence the final metamorphic grain-size. Post-depositional/metamorphic structures include hydrothermal remobilization, brittle deformation (reduces grain size), dynamic recrystallization (reduces grain-size—see Nicholas and Poirier, 1976), pressure-solution, annealing and grain growth.

Second-order factors. These are factors which in general may be considered to have less influence on pyrite grain-sizes than those given above. In some situations, however, second-order factors may assume as much importance as first-order factors. These factors include: the nature of the matrix to the pyrite, whether sulphides or silicates; if silicates, the nature of the grain boundaries of the matrix minerals (for example, the strong planar boundaries of micas or amphiboles will tend to inhibit grain growth perpendicular to that boundary hence appearing to enhance grain growth parallel to the strong planar boundary); grain–grain boundary interference, such as the presence of inclusions pinning grain boundaries during grain growth; replacement of silicates or carbonates by pyrite; and, finally, the chemistry of the pyrite.

In the pyrite examined in this study we have taken care to assess all of the above first and second order factors through the following procedures:

(1) All specimens were carefully etched in 10% HNO_3 in order that growth and deformation features could be assessed and various pyrite phases recognized. We have subdivided the pyrite into two main groups—primary depositional sizes as discussed above and deformation/metamorphic grain-sizes (fig. 3, Table II).

(2) We have attempted, where possible, to identify hydrothermal remobilization which usually forms inclusion-free euhedral grains associated with quartz or carbonate veins.

(3) Second-order factors on grain-sizes and deformation/recrystallization textures have been minimized, where possible, by: using pyrite-rich specimens (> 40% by volume of pyrite); avoiding areas where strong planar silicate boundaries have inhibited grain growth; avoiding areas where inclusions have pinned and inhibited grain boundary migration; and avoiding specimens where strong grain–grain interference has visibly restricted grain growth (particularly in ores which have undergone little deformation). In the samples used for this study little evidence for significant replacement of other phases by pyrite was found.

Electron microprobe analyses of the pyrite have shown little chemical variation or departure from

TABLE II. *Characteristics of pyrite from each deposit studied*

Deposit	Depositional/early diagenetic	Metamorphic
Tom	Fine (20–30 μm) spheroids and subhedral or euhedral diagenetic overgrowths (60–150 μm)	Large (100–800 μm) rarely zoned euhedral crystals
Driftpile	Spheroids (20–100 μm) with subhedral or euhedral diagenetic overgrowths (60–80 μm)	Large (3–4 mm) rarely zoned euhedral crystals containing primary pyrite phases
Cirque	Spheroids (10–50 μm), euhedral diagenetic and colloform overgrowths (50–150 μm)	Large (4–5 mm) brecciated crystals, some undeformed, zoned porphyroblasts (200–300 μm)
Mount Isa	Spheroids (10–20 μm) with euhedral diagenetic overgrowths (20–40 μm)	Large (2–3 mm) euhedral or subhedral crystals overgrowing primary phases
Sullivan	Spheroids (10–20 μm) with subhedral diagenetic overgrowths (50–60 μm) with a 2–3 mm radiating buckshot texture	Weak annealing texture (200–300 μm), some large (5–6 mm) rotated porphyroblasts
Vangorda	No data available	
Reeves MacDonald	Subhedral primary grains (50–300 μm) define an old mineral layering	Large (100–500 μm) annealed crystals
HB	Fine subhedral primary grains up to 100 μm	Large (300–1200 μm) strongly annealed crystals
Faro	Rare primary grains (60–100 μm)	Strongly annealed (200–7500 μm) crystals, minor recrystallization in late shear zones
It	No data available	
King Fissure	No data available	

stoichiometric FeS_2 ($\pm 0.15\%$ Fe and $\pm 0.2\%$ S). The characteristics of pyrite from each deposit are summarized in Table II.

Grain-size distribution

The grain-size data in fig. 3 show two data sets, one for recognizable primary pyrite phases and one for metablastic pyrite.

Primary phases including pyrite spheroids, and small euhedral grains are found in the Tom, Driftpile, Cirque, and Mount Isa deposits. Massive colloform aggregates are found in the Cirque deposit. At all metamorphic grades above those for Vangorda and Sullivan it becomes increasingly difficult to identify primary pyrite textures. Where identified, primary pyrite grains (apart from massive colloform aggregates) are generally less than 100 μm (fig. 3) and commonly 20–40 μm in size.

Metamorphic pyrite grain-sizes exhibit an increase in grain-size with increasing metamorphic grade (fig. 3). The disparities at the low-grade end of the spectrum reflect the difficulty in differentiating between remobilization, colloform-massive primary pyrite and grain growth features (fig. 3).

Pyrite microstructures

The pyrite microstructures from a number of deposits will now be described in detail. In particular, emphasis is placed on those textures found in sulphide deposits in low-grade metamorphic environments. Pyrite microstructures have been studied in both the ores and host rocks and particularly where pyrite is relatively abundant in order that pyrite–pyrite deformation interactions could be assessed. Our observations on the deformation mechanisms of pyrite have not been applied to situations where pyrite occurs as isolated euhedral porphyroblasts in the host rocks. In this latter situation, the pyrite euhedra commonly remain largely undeformed, acting as stress risers (Selkman, 1983) with the development of quartz–carbonate pressure shadows as the host lithology deforms around the pyrite grains.

The textures found in the higher grade metamorphic environments are compared with those found by Templeman-Kluit (1970) and Lawrence (1972). In this paper, attention is focused on deformation and grain growth microstructures. In all examples studied by the authors, diagenetic and 'hydrothermal' remobilization of pyrite was evident but careful detailed study of etched polished sections enabled these features to be distinguished from deformation and recrystallization microstructures.

Pyrite in very low-grade metamorphic environments. The Driftpile, Tom, and Cirque deposits have undergone only very low-grade metamorphism (sub-greenschist facies) probably at temperatures less than 200 °C (fig. 2). Slaty cleavages and spaced pressure-solution cleavages are found in the ores and host rocks (McClay, 1983). In the ore environment, pyrite typically occurs either as massive colloform aggregates or as fine-grained laminae of spheroidal grains from 5 μm–40 μm in size. Pyrite layers are commonly strongly folded with the development of an axial planar fabric (fig. 4*a*). In detail, the fabric is commonly a spaced pressure-solution style cleavage with dark seams of insoluble material (often carbonaceous) defining the fabric.

Small pyrite spheroids and grains are often strongly indented (fig. 4*b*), with the mutual boundary of the spheroids forming part of a cleavage seam. Clear, inclusion-free, euhedral pyrite overgrowths are commonly found in areas of low mean stress adjacent to truncated spheroids (fig. 4*c*). These euhedral pyrite overgrowths are smaller than, or are the same size as, the spheroidal pyrite.

Elsewhere in these deposits pyrite grains, both small and large have undergone strong cataclastic deformation. Micro and mesoscopic shear zones are developed. Spheroidal pyrite is strongly disaggregated. Coarse-grained pyrite (often originally colloform or large euhedral porphyroblasts) typically fractures during deformation.

In the massive ores of the Cirque deposit, for example, spectacular 'blow apart' structures are developed (fig. 4*d*) with remobilized galena infilling the fractures. In this case, a crude fracture cleavage is defined by the pervasive fragmentation of the massive pyritic ores.

Pyrite in low greenschist facies environments. The laminated pyritic shales of the Urquhart Shale Formation in the Mount Isa deposit are, in some areas of the mine, strongly folded (McClay, 1979, 1983). The pyrite laminae display numerous microscopic but penetrative shear zones. In detail, spectacular microstructures are observed. These include disaggregated pyrite grains, spaced cleavages, truncation and indentation of spheroids and euhedral overgrowths. In particular, high strain areas are characterized by strong indentation and truncation of spheroids (fig. 5*a*) and the development of pressure-solution cleavages. Coarse-grained pyrite is commonly brecciated and fragmented but in places strong indentation of one grain upon another is observed (fig. 5*b*). Grain–grain indentation is accompanied by well-developed axial cracking (fig. 5*b*).

Pyrite from mid–upper greenschist facies environments. Examples of pyritic ore deformed in mid–upper greenschist facies are taken from the Reeves MacDonald mine in the Kootenay Arc (fig. 1, Table I) and from the pyritic southeastern fringe of the

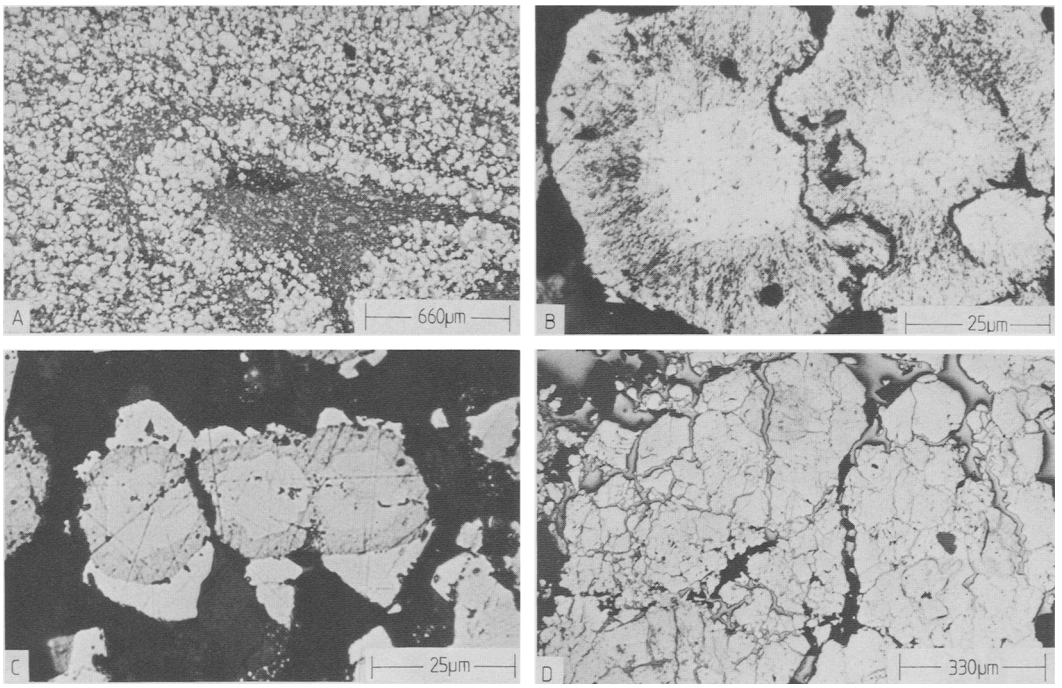

FIG. 4. Microstructures in deformed pyrite. (*a*) Folded pyritic laminae showing a well-developed axial planar foliation. Driftpile deposit. PPL. (*b*) Indented pyrite spheroids showing strong dissolution of fibrous overgrowths along an irregular sub-vertical seam which forms part of a strong vertical spaced cleavage. Driftpile deposit. PPL, oil immersion. (*c*) Pyrite spheroids showing dissolution along sub-vertical seams and the development of inclusion-free pyrite overgrowths in areas of low mean stress. Cleavage is vertical. Driftpile deposit. PPL, oil immersion. (*d*) Strongly fragmented massive pyrite from the Cirque deposit. Fractures are infilled with remobilized galena. PPL.

Sullivan orebody (fig. 1, Table I, Hamilton *et al.*, 1982, 1983). In this part of the Sullivan orebody, deformation is restricted to localized folding and thrust faulting (McClay, 1983). Ductile deformation microstructures (such as slip lines, sub-grains, elongate grains and dynamic recrystallization textures) are not observed in this type of Sullivan ore. Rather, grain growth and brittle deformation features are common. Annealing grain growth microstructures in the pyrite are characterized by euhedral grains and straight grain boundaries, triple points and other phases concentrated along grain boundaries and at triple points (fig. 5*c*). Elsewhere in the Sullivan deposit, the pyrite typically occurs as massive aggregates (generally little deformed), fractured euhedral grains, or as rotated porphyroblasts in a pyrrhotite matrix.

In the Reeves MacDonald deposit, the pyritic layers are commonly strongly folded into tight isoclinal folds. The medium–coarse-grained pyrite (fig. 3) generally exhibits subhedral forms with curved grain boundaries, triple points and inclusions of other phases trapped at grain boundaries or at triple junctions. In places, grains are fractured but no sub-grains or dislocation features were identified.

Pyrite in amphibolite-facies environments. Both the Faro orebody (Templeman-Kluit, 1970) and the HB deposit (Fyles, 1970) contain significant pyrite. In both deposits it is predominantly coarse-grained (fig. 3), although in the Faro deposit, rare small grains enclosed in coarser pyrite have been observed. Grain growth/annealing textures abound with triple points and straight to lobate grain boundaries developed (fig. 5*d*). Strong grain growth is evident from the abundant inclusions of sphalerite and silicates in the metablastic pyrite and, in places, pinned grain boundaries have inhibited grain growth. In the Faro deposit, later deformation has produced localized shear zones with strong fracturing and localized dislocation movement particularly with high stresses at crack tips.

Discussion

Grain-sizes. The grain-size data (fig. 3) show that, for the deposits in this study deformed up

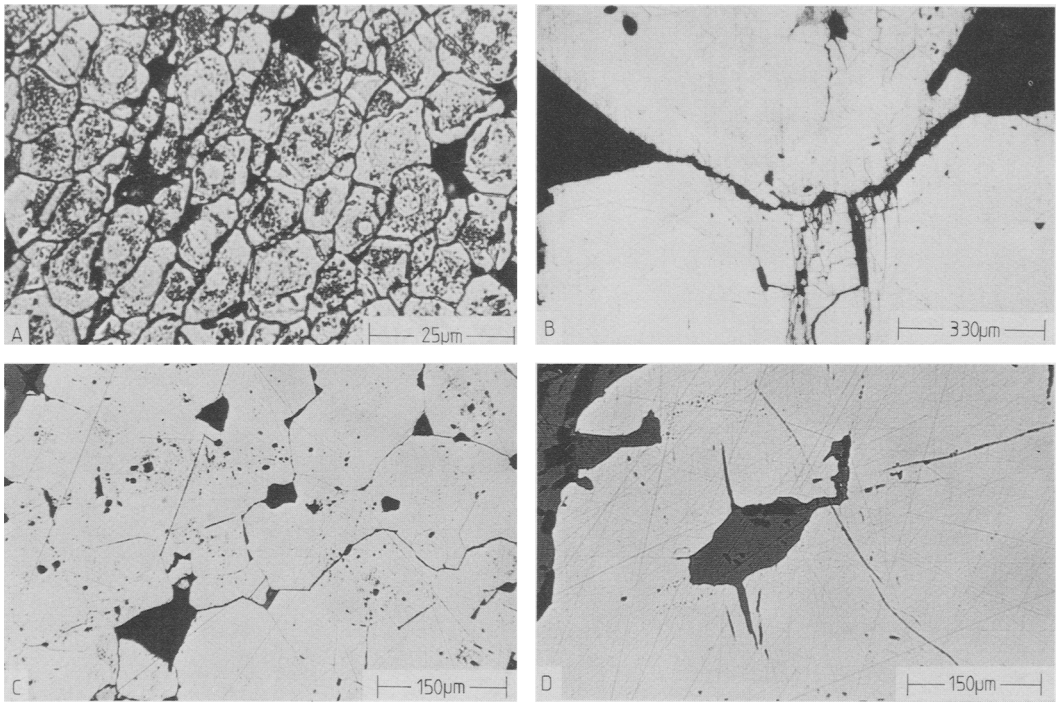

FIG. 5. Pyrite microstructures. (*a*) Strongly indented and elongate pyrite spheroids showing partial dissolution and the development of a penetrative cleavage fabric. Mount Isa deposit. PPL, oil immersion. (*b*) Indentation of large euhedral pyrite showing lattice bending and marked axial cracking. Mount Isa deposit. PPL. (*c*) Annealing texture showing equant grains with triple junctions and straight grain boundaries. Silicates are trapped at grain boundaries or at triple points. Sullivan deposit, 3667 cross-cut, PPL. (*d*) Grain growth texture from the Faro deposit showing a large pyrite porphyroblast which has enveloped a sphalerite grain (the sphalerite was probably originally trapped at a triple point). Note the pyrite growing into the sphalerite matrix at the upper left of the photograph. PPL.

to mid-greenschist facies, primary depositional/diagenetic grain-sizes are generally less than 80 μm (colloform textures excepted), typically 20–40 μm in size. Metamorphic pyrite generally shows an increase in grain-size with an increase in metamorphic grade (fig. 3) similar to that found by Templeman-Kluit (1970).

Deformation textures. In low-grade metamorphic environments, fragmentation, axial cracking and pressure-solution textures predominate (Tom, Driftpile, Cirque, and Mount Isa). Primary microstructures become disaggregated and pyrite pressure-solution overgrowths developed. Spaced cleavages comprising seams of insoluble material are commonly well developed (Cirque and Mount Isa deposits).

At higher metamorphic grades, annealing (Lawrence, 1972) or grain growth textures predominate (Sullivan and Reeves MacDonald). Little evidence of dynamic recrystallization—sub-grains, high dislocation densities, elongate grains or preferred orientations—have been found in the examples studied. At the highest metamorphic grades studied (Faro), coarse grain-sizes predominate and there is abundant evidence of grain growth. At these high temperatures one would expect grain growth to rapidly heal earlier formed fractures, perhaps only leaving a trail of included phases (e.g. sphalerite and silicates) to indicate that brittle deformation has occurred.

The deformation textures found in this study are summarized in fig. 6. The boundaries between the various fields on the diagram must be regarded as transitional (note that the vertical axis is not to scale).

Deformation mechanisms. Careful study of the pyrite in these deformed sulphide orebodies has enabled the following deformation mechanisms to be identified.

(1) Cataclasis or brittle failure has been found in most specimens studied. It is, however, predominant at low metamorphic grades, particularly in the

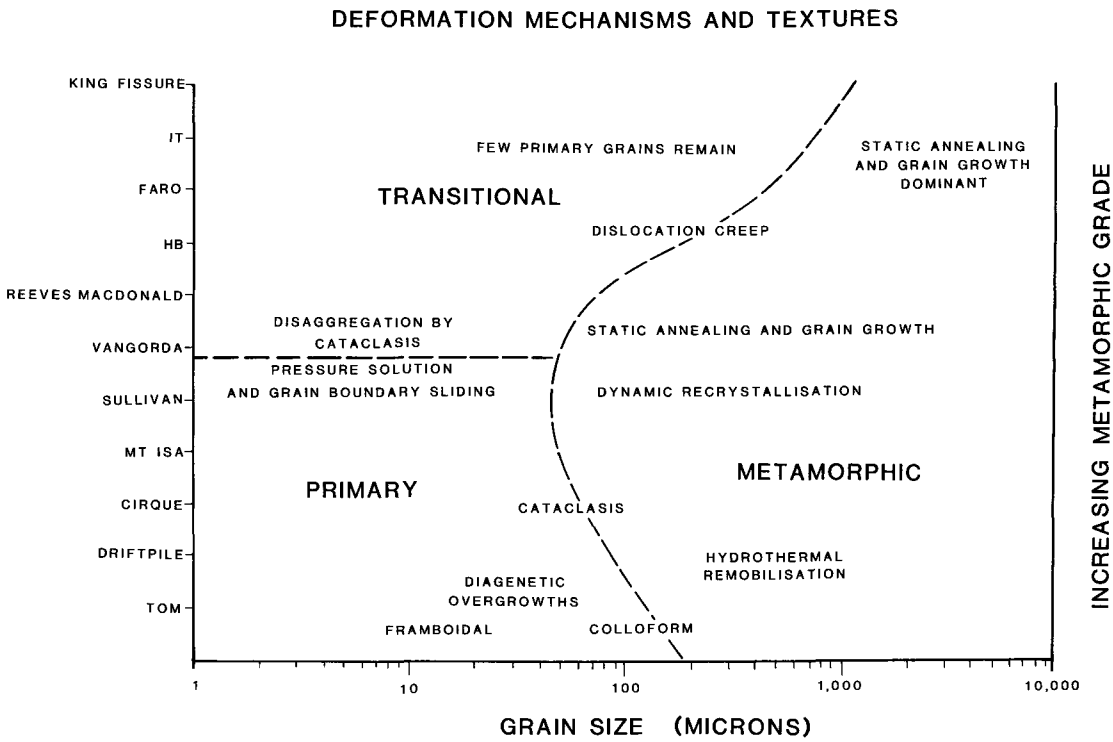

FIG. 6. Summary of the deformation textures and mechanisms as observed in this study. The boundaries are transitional. also note that the vertical axis is not to scale.

coarser grain-sizes. Axial cracking, possibly along the (001) or (110) planes is common. Brittle failure induces fragmentation and grain-size reduction.

(2) Pressure-solution and concomitant grain boundary sliding (necessary to prevent a volume increase—Raj and Ashby, 1971; Ashby and Verrall, 1973) is a major deformation mechanism in fine-grained pyritic ores at low metamorphic grades. Pressure-solution overgrowths are typically of the same order of magnitude in size as the grains undergoing deformation. Pressure-solution is common in shear zones or cleavage bands. Remobilization by pressure-solution may be a possible mechanism for the formation of elongate pyrite grains in some deformed ores (Sarkar *et al.*, 1980).

(3) There is little evidence of dynamic recrystallization in the pyritic ores used in this study. That is not to say, however, that the pyrite has not deformed by dislocation movement because experimental evidence (Cox *et al.*, 1981) permits one to infer that pyrite should deform by dislocation processes at medium-high metamorphic grades.

(4) Grain growth/annealing is a dominant mechanism at medium-high metamorphic grades. It is likely that this very strong grain growth has obliterated evidence of any earlier cataclastic deformation and/or any earlier intracrystalline plasticity. It may also be expected that pyrite grain growth would continue during uplift, once deformation ceased, and that grain growth would continue until the attainment of a sufficiently low temperature at which the rate of grain growth was so slow as to effectively cease.

The relationships between initial grain-sizes, cooling rates and stable grain-sizes warrants detailed laboratory investigations.

Deformation mechanism maps. The deformation of pyrite may be illustrated by means of a deformation mechanism map (Frost and Ashby, 1982) which displays the relationship between flow stress, strain-rate, temperature, and grain-size (see Atkinson, 1977, or Frost and Ashby, 1982, for details).

A schematic deformation mechanism map for pyrite of 100 μm grain-size is shown in fig. 7. The brittle/ductile transition is constrained by the experimental data from Atkinson (1972, 1975) and

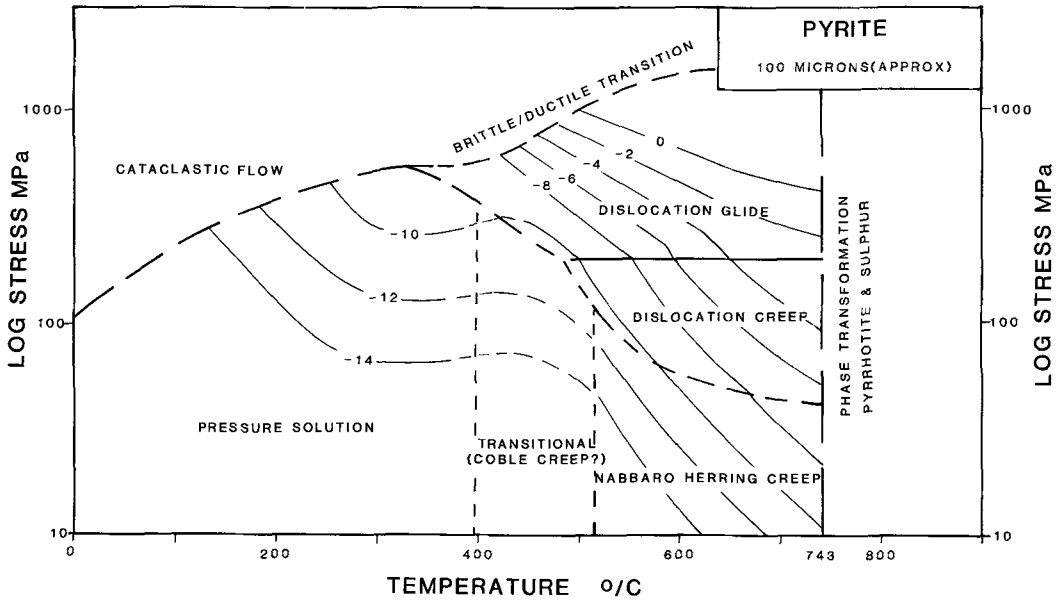

FIG. 7. Deformation mechanism map for 100 μm pyrite which has been constructed using the experimental data from references cited in the text and based upon observations in naturally deformed pyrite. The contours on the diagram are strain-rates in units of 10^{-n} sec^{-1}.

Cox *et al.* (1981) whereas the strain-rate contours for dislocation glide and creep were constructed using the data from Cox *et al.* (1981). The strain-rate contours for diffusion deformation, Coble Creep and Nabarro–Herring Creep, are schematic, based upon estimations of natural deformation rates for the deposits used in this study. The estimated stress levels are high, 10–100 MPa (compared with those for galena, see Atkinson, 1977) because in most naturally deformed pyritic ores, brittle failure has occurred. The deformation fields in which one particular mechanism dominates are shown in fig. 7.

At geological strain-rates (10^{-12} to 10^{-14} sec^{-1}) pressure-solution with concomitant grain boundary sliding is a dominant mechanism in low-grade metamorphic environments. Dislocation creep and dislocation glide occur at high stress levels, high temperatures and at fast strain-rates (10^{-8} to 10^{-4} sec^{-1}) under experimental conditions (Cox *et al.*, 1981), whereas diffusional creep–Coble creep or Nabarro–Herring creep (see McClay, 1977 for a review of these mechanisms) are expected to operate at high temperatures but a lower strain-rate (fig. 7).

The deformation mechanism map does not, however, incorporate grain growth and annealing which, as discussed above, would tend to obliterate any evidence of dislocation glide or creep in pyritic ores deformed at high metamorphic grades (e.g. HB or Faro deposits).

Conclusions

This study has demonstrated that the pyrite in metamorphosed stratiform sediment-hosted Pb–Zn deposits increases in grain-size with increasing metamorphic grade. Primary depositional and diagenetic textures in pyrite are preserved at grades up to mid-upper greenschist facies metamorphism. At higher metamorphic grades only metablastic pyrite grains have been observed.

Cataclasis, pressure-solution and annealing/grain growth are the major mechanisms which affect the deformation and textural development of pyrite. Brittle deformation is found at all metamorphic grades and is most prevalent in coarse-grained pyrite in low-grade metamorphic environments. Textural evidence of truncated spheroids, indented grains, overgrowths and spaced cleavages permits one to infer that pressure-solution and grain boundary sliding are major deformation mechanisms in fine-grained pyritic ores in low-grade metamorphic environments. This may give rise to elongate pyrite grains and a pyrite linear fabric. At higher metamorphic grades grain growth/annealing dominates, probably destroying any evidence of either cata-

clastic or dislocation deformation. Evidence of dislocation glide has only been found in zones of intense shearing and brittle deformation where high shear stresses at crack tips promotes dislocation movement.

Significant macroscopic ductility of pyritic ores in low-grade metamorphic environments may be achieved by a combination of cataclastic flow and pressure-solution, particularly favoured by small pyrite grain-sizes. At higher temperatures, recrystallization and grain growth compete with these deformation mechanisms so much so that the pyrite grain-size increases and these coarse-grained ores appear to deform either by cataclasis or, in part, by dislocation creep which may be masked by later annealing.

Acknowledgements. K. R. McClay's research on the deformation of stratiform sulphide deposits of the Canadian Cordillera has been generously supported by Goldsmith's College Research Grants. The visit to the Faro deposit was supported by a Royal Society Travel Grant. Field work was greatly facilitated by Cominco, Cyprus Anvil Mining Corporation and Hudsons Bay Exploration and Development. Material and information on the Driftpile deposit was provided by R. Carne. P. Ellis's research was carried out at Imperial College whilst in receipt of a NERC Postgraduate Studentship. Mr T. Easter is thanked for assistance with photography.

REFERENCES

Adams, F. D. (1910) *J. Geol.* **35,** 489–535.
Arnold, M. (1978) Unpub. Theses Doctoral es-Sciences. Nancy.
Ashby, M. F., and Verrall, R. A. (1973) *Acta. Metall.* **21,** 149–63.
Atkinson, B. K. (1972) Unpub. Ph.D. thesis, University of London. 252 pp.
——(1975) *Econ. Geol.* **70,** 473–87.
——(1977) *Geol. Foren. Stockh. Forh.* **99,** 186–97.
Barnes, H. L., and Czamanske, G. K. (1967) In *Geochemistry of Hydrothermal Ore Deposits* (H. L. Barnes, ed.) Rinehart and Winston, New York, 334–81.
Bridgman, P. W. (1937) *Proc. Am. Acad. Arts. Sci.* **71,** 387–460.
Buerger, M. J. (1928) *Am. Mineral.* **13,** 35–51.
Campbell, F. A., and Ethier, V. G. (1974). *Econ. Geol.* **69,** 482–93.
Couderc, J.-J., Bras, J., Fagot, M., and Levade, C. (1980) *Bull. Mineral.* **103,** 547–57.
Cox, S. F., Etheridge, M. A., and Hobbs, B. E. (1981) *Econ. Geol.* **76,** 2105–18.
Davis, G. H. (1972) Ibid. **67,** 634–55.
Frost, H. S., and Ashby, M. F. (1982) *Deformation mechanism maps. The plasticity and creep of metals and ceramics.* Pergamon, Oxford. 166 pp.
Fyles, J. T. (1970) *British Columbia Department of Mines and Petroleum Resources.* Bull. **57,** 64 pp.
——and Hewlett, C. G. (1959) *British Columbia Department of Mines* Bull. **41,** 162 pp.
Gay, N. C. (1970) *J. Geol.* **78,** 523–32.
Graf, J. L., Jr., and Skinner, B. J. (1970) *Econ. Geol.* **65,** 206–15.
——————Bras, J., Fagot, M., Levade, C., and Courderc, J.-J. (1981) Ibid. **76,** 738–44.
Hamilton, J. M., Bishop, D. T., Morris, H. C., and Owens, O. E. (1982) In *H. S. Robinson Memorial Volume* (R. W. Hutchinson, ed.). Geol. Assoc. Can. Special Paper 25, 597–665.
——Delaney, G. D., Hauser, R. L., and Ransom, P. W. (1983) In *Sediment-Hosted Stratiform Lead–Zinc Deposits.* Short Course Notes. Mineral. Assoc. Can. 31–72.
Höy, T. (1982) In *H. S. Robinson Memorial Volume* (R. W. Hutchinson, ed.) Geol. Assoc. Can. Special Paper 25, 127–47.
Jefferson, C. W., Kilby, D. B., Pigage, L. C., and Roberts W. J. (1983) In *Sediment-Hosted Stratiform Lead–zinc Deposits.* Short Course Notes. Mineral. Assoc. Can. 121–39.
Lang, H. (1968) Unpub. Dissertation, Rheinisch–Westfalisch Technische Hochschule, Aachen. 131 pp.
Large, D. E. (1980) *Geol Jahrb.* **40,** 59–130.
Lawrence, L. J. (1972) *Econ. Geol.* **67,** 487–96.
Levade, C., Couderc, J.-J., Bras, J., and Fagot, M. (1979) *Phil. Mag.* A, **40,** 111–20.
McClay, K. R. (1977) *J. Geol. Soc. Lond.* **134,** 57–70.
——(1978) Unpub. Ph.D. thesis, University of London. 454 pp.
——(1979) *Trans. Inst. Mining Metall.* **88,** B5–B14.
——(1982) In *Atlas of Deformational and Metamorphic Rock Fabrics* (G. J. Borradaile, M. B. Bayly, and C. McA. Powell, eds.). Springer-Verlag, Berlin. 374–83.
——(1983) In *Sediment-Hosted Stratiform Lead–Zinc Deposits.* Short Course Notes. Mineral. Assoc. Can. 283–307.
MacIntyre, D. (1979) *Geological Fieldwork 1979.* British Columbia Ministry of Energy, Mines and Petroleum Res., 56–67.
Masalovich, A. M. (1977) *Internat. Geol. Rev.* **19,** 208–16.
Mathias, B. V., and Clarke, G. J. (1975) In *Economic Geology of Australia and Papua-New Guinea.* **1,** Metals. (C. L. Knight ed.) Austral. Inst. Mining Metall. 351–72.
Mookherjee, A. (1971) *Econ. Geol.* **66,** 200.
——(1976) In *Handbook of Stratabound and Stratiform Ore Deposits* K. H. Wolf, ed.) Elsevier, Amsterdam. **4,** 203–60.
Natale, P. (1971) *Rend. Soc. Italian Miner. Petrol.* **27,** 539–50.
Newhouse, W. H., and Flaherty, G. F. (1930) *Econ. Geol.* **25,** 600–4.
Nicholas, A., and Poirier, J. P. (1976) *Crystalline Plasticity and Solid State Flow in Metamorphic Rocks.* Wiley, London. 444 pp.
Raj, R., and Ashby, M. F. (1971) *Met. Trans.* **2,** 1113–27.
Ramdohr, P. (1969) *The Ore Minerals and Their Intergrowths.* Pergamon, Oxford. 1174 pp.
Robertson, E. C. (1955) *Geol. Soc. Am. Bull.* **66,** 1275–314.
Rozendaal, A. (1978) In *Mineralisation in Metamorphic Terranes* (W. J. Voerwoerd, ed.), Geol. Soc. S. Africa Spec. Publ. **4,** 235–68.
Sarkar, S. C., Bhattacharyya, P. K., and Mukherjee, A. D. (1980) *Econ. Geol.* **75,** 1152–67.

Selkman, S. O. (1983) *J. Structural Geology* **5,** 47–52.
Templeman-Kluit, D. J. (1970) *Can. J. Earth Sci.* **7,** 1339–45.
Van Goethem, L., Van Landuyt, J., and Amelinckx, S. (1978) *Am. Mineral.* **63,** 548–50.
Vokes, F. M. (1969) *Earth Sci. Rev.* **5,** 99–143.
——(1971) *Mineral. Deposita,* **6,** 122–9.
——(1976) In *Handbook of Stratabound and Stratiform Ore Deposits* (K. H. Wolf, ed.). Elsevier, Amsterdam. **6,** 79–127.

[*Revised manuscript received 13 June 1983*]